Journal of ELECTRONIC MATERIALS, Vol. 45, No. 7, 2016
DOI: 10.1007/s11664-016-4502-9
© 2016 The Author(s). This article is published with open access at Springerlink.com

Resonant Levels, Vacancies, and Doping in Bi_2Te_3, Bi_2Te_2Se, and Bi_2Se_3 Tetradymites

BARTLOMIEJ WIENDLOCHA[1,2]

1.—Faculty of Physics and Applied Computer Science, AGH University of Science and Technology, Aleja A. Mickiewicza 30, 30-059 Kraków, Poland. 2.—e-mail: wiendlocha@fis.agh.edu.pl

The electronic structure of the tetradymites, Bi_2Te_3, Bi_2Te_2Se, and Bi_2Se_3, containing various dopants and vacancies, has been studied using first-principles calculations. We focus on the possibility of formation of resonant levels (RL), confirming the formation of RL by Sn in Bi_2Te_3 and predicting similar behavior of Sn in Bi_2Te_2Se and Bi_2Se_3. Vacancies, which are likely present on chalcogen atom sites in real samples of Bi_2Te_2Se and Bi_2Se_3, are also studied and their charged donor and resonant behavior discussed. Doping of vacancy-containing materials with regular acceptors, such as Ca or Mg, is shown to compensate the donor effect of vacancies, and $n-p$ crossover, while increasing the dopant concentration, is observed. We verify that the RL on Sn is not disturbed by chalcogen vacancies in Bi_2Te_2Se or Bi_2Se_3, and for the Sn-doped materials with Se or Te vacancies, double doping, instead of heavy doping with Sn, is suggested as an effective way of obtaining the resonant level. This should help to avoid smearing of the RL, a possible reason for earlier unsuccessful experimental observation of the influence of the RL on the thermoelectric properties of Sn-doped Bi_2Te_2Se. Finally, we show that Al and Ga are possible new resonant impurities in tetradymites, hoping that this will stimulate further experimental studies.

Key words: Tetradymites, resonant levels, thermoelectrics

INTRODUCTION

The tetradymites are a group of minerals with general formula $(Bi,Sb)_2(Te,Se)_3$, intensively studied as thermoelectric materials for operation near room temperature, for Peltier cooling or power generation applications,[1] and more recently as topological insulators (TI).[2–4] The best known material from this family is Bi_2Te_3, whose alloys have a large thermoelectric figure of merit, ZT, of around 1.0 near room temperature,[1] while the best tetradymite alloys and nanocomposites even reach ZT = 1.5 around $T = 400$ K.[5] In this work, we focused on the electronic structure of the bismuth-based tetradymites, Bi_2Te_3, Bi_2Te_2Se, and Bi_2Se_3, containing impurity atoms and vacancies. The band structure of the pure compounds is quite well known, both theoretically and experimentally (see Refs. 6–14 and references therein). However, much less theoretical work has been devoted to the electronic structure of materials with defects or impurities, especially compared with, e.g., the lead telluride family, which is likely related to the more complicated crystal structure of the tetradymites. This was one of the motivations for this work, and our aim was to systematically study the main features of the electronic structure of tetradymites containing various dopant atoms and vacancies. We focus on so-called resonant impurities, starting with Sn in Bi_2Te_3 as already investigated experimentally, and extending those studies to the other two materials. The second aspect of the present work is to shed more light on the behavior of vacancies in Bi_2Se_3 and Bi_2Te_2Se, and their effect on the possibility of RL formation. The chemistry of defects in Bi_2Te_3 is

(Received January 19, 2016; accepted March 28, 2016; published online April 20, 2016)

much better known and controlled,[15] thus we discuss the two other materials, which are naturally n-type, for which vacancies[2] (on either Se or Te) are often considered responsible. We explore whether the presence of vacancies may alter the formation of the resonant state on Sn, and verify whether double doping with already known effective p-type impurities (Ca and Mg) may be an efficient way of tuning the Fermi level position in Sn-doped material, as an alternative to heavy doping with Sn. Finally, we propose two new, potentially interesting impurities, which may form resonant levels in tetradymites, namely Al and Ga, to stimulate further experimental work on this family of materials.

COMPUTATIONAL DETAILS

All three studied compounds, Bi_2Te_3, Bi_2Te_2Se, and Bi_2Se_3, crystallize with rhombohedral structure[2,16] in space group no. 166, $R\text{-}3m$, consisting of a sequence of atomic layers, Te(1)–Bi–Te(2)–Bi–Te(1) (Bi_2Te_3), Te(1)–Bi–Se(2)–Bi–Te(1) (Bi_2Te_2Se), and finally Se(1)–Bi–Se(2)–Bi–Se(1) (Bi_2Se_3). This sequence of five layers is often called a quintuple layer; atoms within the layer are covalently bounded, whereas between the quintuple layers there are weaker, van der Waals bonds.[2,13] Experimental unit cell parameters and atomic positions, for each of the structures, are gathered in Table I, and these values were used in calculations performed in this work. In the unit cell of tetradymites, atoms occupy three nonequivalent crystal sites. Bi and Te(1)/Se(1) are located at $2c$ sites, with coordinates (x, x, x), whereas Te(2)/Se(2) atoms are placed at $1a$, i.e., (0,0,0), position.

Electronic structure calculations were carried out within the density functional theory (DFT) formalism. The Korringa–Kohn–Rostoker (KKR) method was used[17–19] in the semirelativistic and spherical potential approximations, which are sufficient to describe the density of states or the formation of resonant levels. Chemical disorder, caused by the presence of impurity atoms or vacancies, was simulated using the coherent potential approximation (CPA).[17,18,20] In this approach, using Green function techniques, the real disordered system (e.g., binary alloy A_xB_{1-x}) is replaced by an ordered system of effective "CPA atoms," described by an effective Green function. This effective Green function is calculated self-consistently, employing the CPA condition, in which replacing one of the "CPA atoms" by component A or B atom does not lead to additional scattering or change the averaged properties of the medium. CPA allows one to consider very small impurity concentrations, as low as $x = 0.1\%$, and all calculations for $0 \leq x \leq 1$ use the same primitive cell of the host material. However, such computations in a single unit cell do not allow one to study the crystal structure relaxation process around impurities or vacancies, thus any relaxation effects are neglected in our computations. To obtain the Fermi level position in the doped materials with high accuracy, the Lloyd formula was used.[17] Local density approximation (LDA) was used, with the parametrization of von Barth and Hedin.[21] Very dense k-point meshes for self-consistent cycle and density of states calculations were used, up to ~4600 points in the irreducible part of the Brillouin zone. To increase the unit cell filling, empty spheres with atomic number $Z = 0$ were added between each of the atomic layers.

For the selected case of Sn-doped Bi_2Te_3, additional calculations were performed, using the supercell technique and the full-potential linearized augmented plane-wave method (FP-LAPW, WIEN2k code).[22] This was done to verify whether effects neglected within the KKR–CPA approach (nonspherical potential, crystal lattice relaxation after Sn/Bi atomic substitution, or spin–orbit coupling) may wash out the resonant state. As the answer was negative and RL formation was confirmed in the relaxed FP-LAPW + spin–orbit case (see below), one may expect that the main conclusions of this work, related to the presence of RL, do not depend on crystal structure relaxation or spin–orbit interaction.

RESULTS AND DISCUSSION

Sn Resonant Level

We start our discussion with the very intriguing case of Sn as acceptor in Bi_2Te_3. Sn was found to be a so-called resonant impurity in Bi_2Te_3,[23–25] being a special case of impurity behavior in semiconductors. From the viewpoint of band-structure calculations,

Table I. Experimental[2,13,16] unit cell parameters of Bi_2Te_3, Bi_2Te_2Se, and Bi_2Se_3 in the rhombohedral convention of the unit cell: lattice constant, a (Å), and rhombohedral angle, α_{Rh} (°)

Parameter	Bi_2Te_3	Bi_2Te_2Se	Bi_2Se_3
a (Å)	10.473	10.230	9.841
α_{Rh} (°)	24.16	24.25	24.27
x_{Bi}	0.400	0.3958	0.399
$x_{Te(1)/Se(1)}$	0.2095	0.2118	0.206
$x_{Te(2)/Se(2)}$	0	0	0

Space group no. 166, $R\text{-}3m$, x is the parameter of the $2c$ (x, x, x) site, occupied by Bi and Te(1)/Se(1); Te(2)/Se(2) atoms occupy $1a$ site, with coordinates (0, 0, 0).

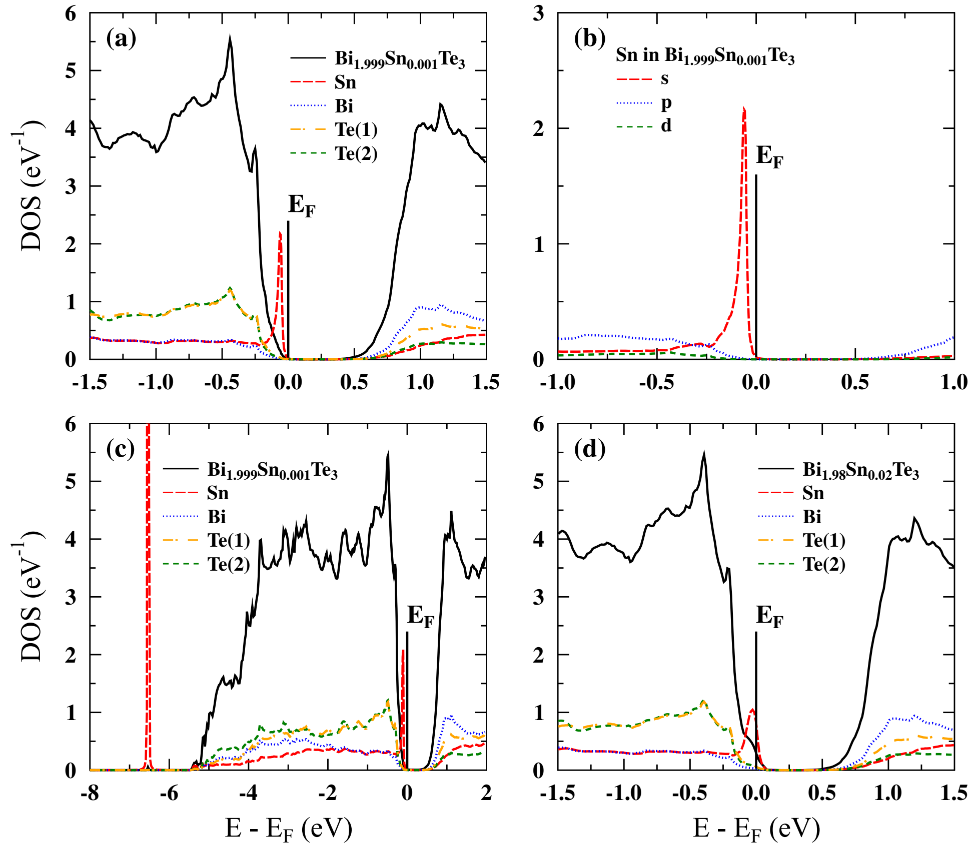

Fig. 1. Calculated DOS of $Bi_{2-x}Sn_xTe_3$: (a–c) $x = 0.001$, (d) $x = 0.02$. Panels (a) and (d) show the total DOS for $E = E_F \pm 1.5$ eV; panel (b) shows the partial Sn DOS with angular momentum decomposition; panel (c) shows the DOS in a broader energy range to show the hyperdeep DOS peak of Sn, around -6.5 eV below E_F. For all the panels and all other figures in this work, the total DOS (solid black line) is given per formula unit, whereas partial atomic densities of states, plotted with colors, are given per single atom, not multiplied by its concentration.

the fingerprint of such a resonant level, also called a virtual bound state,[26–28] is a narrow peak in the density of electronic states (DOS) of the impurity atom at the resonance energy, when the concentration of the impurity atoms is very small (here we use 0.1% to identify RL formation). Due to the presence of such a peak, the doped system, containing resonant impurities, does not follow the rigid-band model,[29–32] where doping would lead to a rigid shift of the Fermi level only. The RL can have various effects on the electronic and transport properties of the material, depending on its details, e.g., position relative to the band edges, orbital momentum quantum number, or degree of hybridization with host crystal states. To list several examples, the RL may: be a charge trap, when it is in the gap of the semiconductor (e.g., indium in PbTe at room temperature[27]); be a strong resonant scattering center, as in the case of transition metal–noble metal alloys;[28] or form defect states which pin the Fermi level and lead to partial charge localization (e.g., $3d$ states of Ti in the conduction band of PbTe).[30,33] All these possibilities can be very interesting subjects for various physical and chemical studies. From the point of view of thermoelectric materials based on semiconductors, the most interesting is the case where the RL is close to the band edge (and thus near the Fermi level) and (partly) hybridizes with host electronic states, causing redistribution of the electronic states around a valence (or conduction) band, which may lead to enhancement of the thermopower (S) and thermoelectric power factor (PF). Such an example is PbTe doped with Tl,[34] where the presence of the RL leads to an increase in the thermopower (from 50 μV/K to 55 μV/K to become 120 μV/K to 140 μV/K) around carrier concentration of $p \approx 5 \times 10^{19}$ cm^{-3} to 10×10^{19} cm^{-3}.[34,35] This increase in thermopower may be understood as an effect of the distortion and increase in the DOS near E_F, created by the resonant peak in the DOS,[27,34] or as recently shown,[29] compared with the effect of the increase in band degeneracy, since the presence of the RL leads to an increase of the number of electronic states available around the valence band, without forming an isolated impurity band.[29]

Other examples of successful realization of the idea of improving the thermoelectric efficiency using a RL are PbTe:Tl alloyed with Si,[36] Se, and S,[35] SnTe:In,[37] or Bi_2Te_3:Sn,[25] which we focus on now.

In p-type $Bi_{2-x}Sn_xTe_3$, for $x \simeq 1\%$ to 2% ($p \approx 3 \times 10^{19}$ cm^{-3} to 6×10^{19} cm^{-3}) at room temperature,

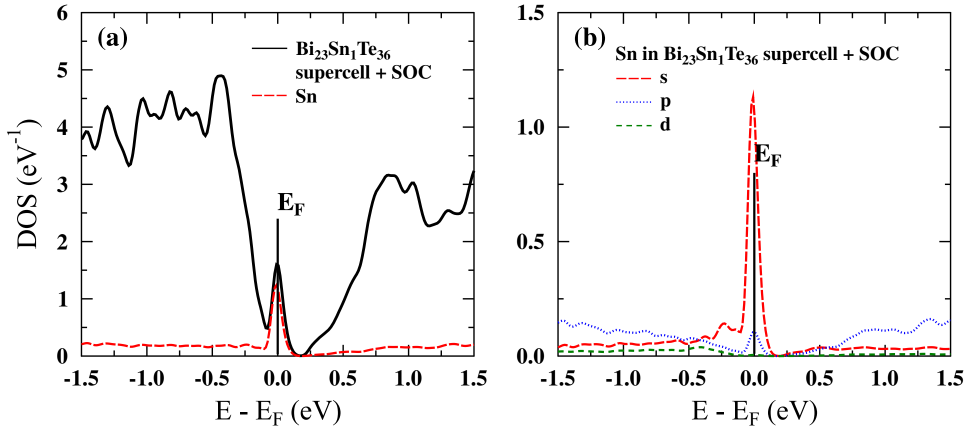

Fig. 2. DOS of the relaxed $Bi_{23}Sn_1Te_{36}$ supercell, computed with spin–orbit coupling taken into account. (a) Black solid line: total DOS, divided by 12 (the number of Bi_2Te_3 formula units in the supercell); red dashed line: Sn atomic DOS; (b) angular momentum decomposition of the Sn atomic DOS. RL is not removed by either the crystal structure relaxation or the spin–orbit interaction (Color figure online).

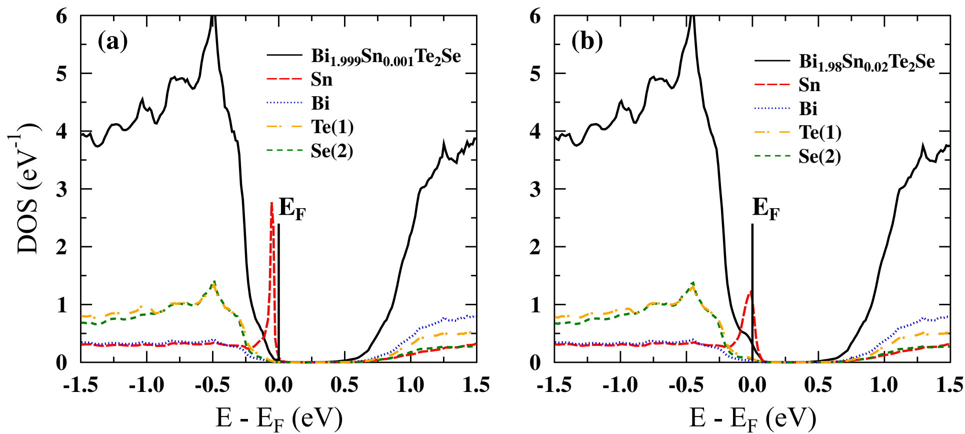

Fig. 3. DOS of $Bi_{2-x}Sn_xTe_2Se$: (a) $x = 0.001$, (b) $x = 0.02$. The RL DOS peak of Sn atom is clearly visible.

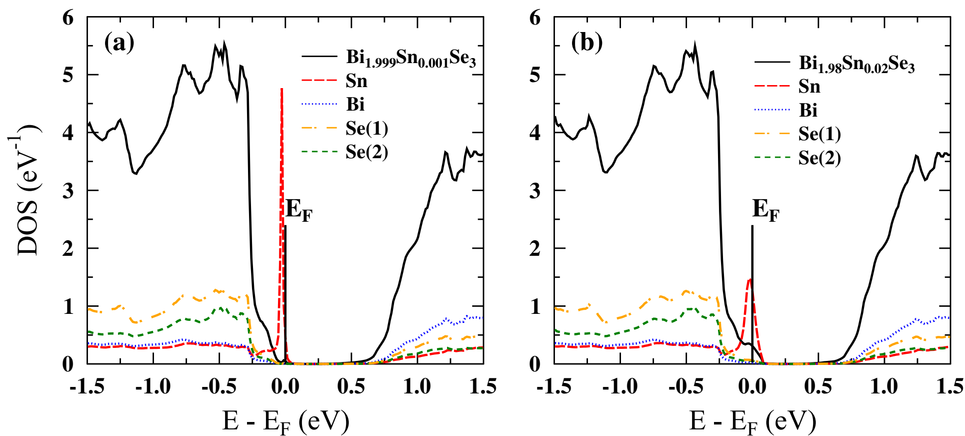

Fig. 4. DOS of $Bi_{2-x}Sn_xSe_3$: (a) $x = 0.001$, (b) $x = 0.02$. The RL DOS peak of Sn atom is clearly visible.

the thermopower was found to be about two times larger (210 μV/K to 220 μV/K) than achieved at the same carrier concentrations but using different acceptors (100 μV/K to 140 μV/K for Pb- or Ge-doped samples). This increase, based also on earlier studies (see Refs. 23–25 and references therein), was explained as due to the formation of the resonant level by Sn atoms. For larger Sn

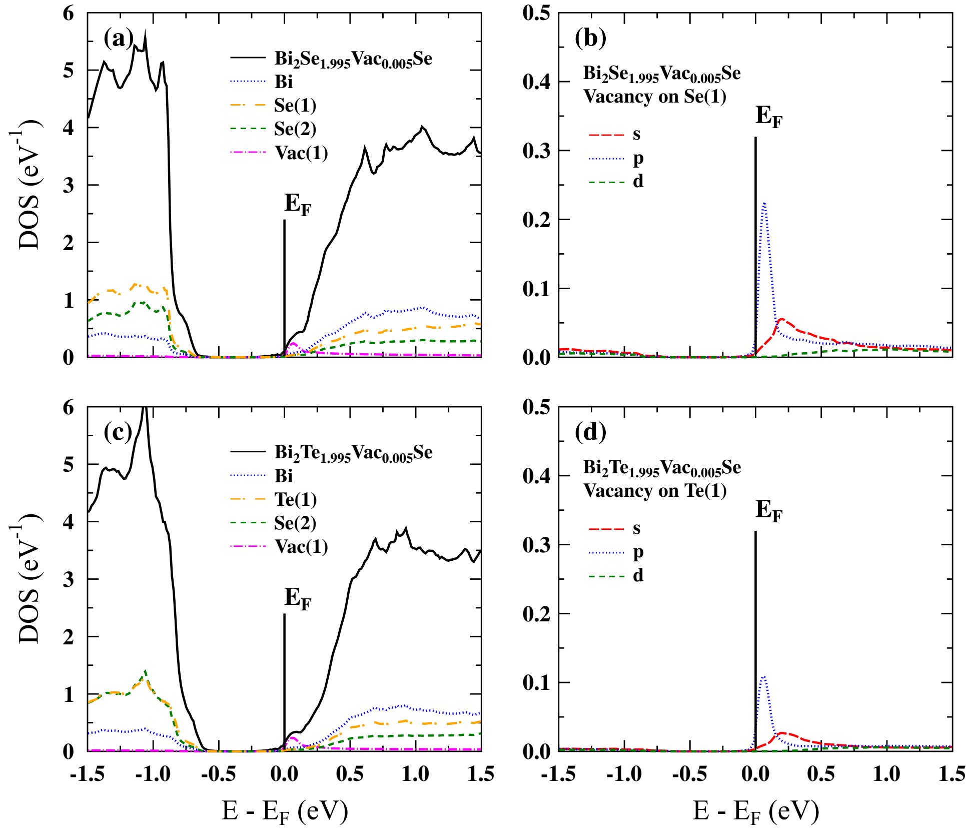

Fig. 5. Vacancies in the "outer" (van der Waals) layer: (a) total DOS of $Bi_2Se_{2.995}$ containing 0.5% vacancies on Se(1), 2*a* crystal sites, (b) partial DOS at vacancy, decomposed over angular momentum; (c, d) as for (a, b) but for the $Bi_2Te_{1.995}Se$ case, containing 0.5% vacancies on Te(1) atom sites.

concentrations ($x = 5\%$), the efficiency of the RL was diminished and S was brought back close to the Pisarenko relation (S versus carrier concentration) for "regular" Bi_2Te_3. Such a loss in RL efficiency for larger Sn concentrations may be related to two factors: First is the possible departure of E_F from the optimal position that maximized the thermopower; as Sn dopes the system p-type, it also controls the position of E_F. Second is smearing of resonant states; as the impurity concentration increases, the level of hybridization with the host band structure becomes larger and the RL broadens, gradually losing its "resonant" character, being integrated into the host electronic structure. This also reduces the height of the DOS peak connected to the RL, as presented below.

Our KKR–CPA electronic structure calculations confirmed the formation of the RL by Sn in Bi_2Te_3, as presented in Fig. 1. Figure 1a–c shows the DOS for the $x = 0.001$ doping case. One can clearly see that Sn forms a sharp, resonant DOS peak near the edge of the valence band (and E_F). In Fig. 1b, the partial Sn DOS is plotted, with angular momentum decomposition. The orbital momentum character of this DOS peak is mainly s-like, thus the RL is formed by the 5s orbitals of tin. Sn plays a double role in Bi_2Te_3, as it also dopes the system p-type: when the concentration of Sn atoms is increased, E_F moves deeper into the valence band (Fig. 1d). At the same time, the resonant peak broadens and hybridizes with the valence-band DOS. Figure 1c shows the DOS for a larger energy range, where one can see that Sn in Bi_2Te_3 creates two resonant levels: one at the valence band edge, and a second one, a so-called hyperdeep defect state (HDS),[38] at −6.5 eV below E_F [in this terminology, the RL near the valence band edge is called a deep defect state (DDS)]. This state is also s-like, and these two resonant states usually appear together, as the analog of a bonding–antibonding pair of orbitals. A similar situation was found for group III impurities (Tl, In, Ga) in PbTe.[39,40] It is worth mentioning here that, recently, the formation of a sole HDS (without a DDS near E_F) was found to be a reason for the acceptor behavior of In, Ga, and Sn in elemental bismuth, in spite of the isovalent character of In and Ga with Bi, and this was proposed to be a novel doping mechanism in solids.[41]

As mentioned above, to verify whether effects neglected within the KKR–CPA approach (non-spherical potential, crystal lattice relaxation after Sn/Bi atomic substitution, or spin–orbit coupling) may wash out the resonant state, complementary FP-LAPW computations, using the WIEN2k code,[22]

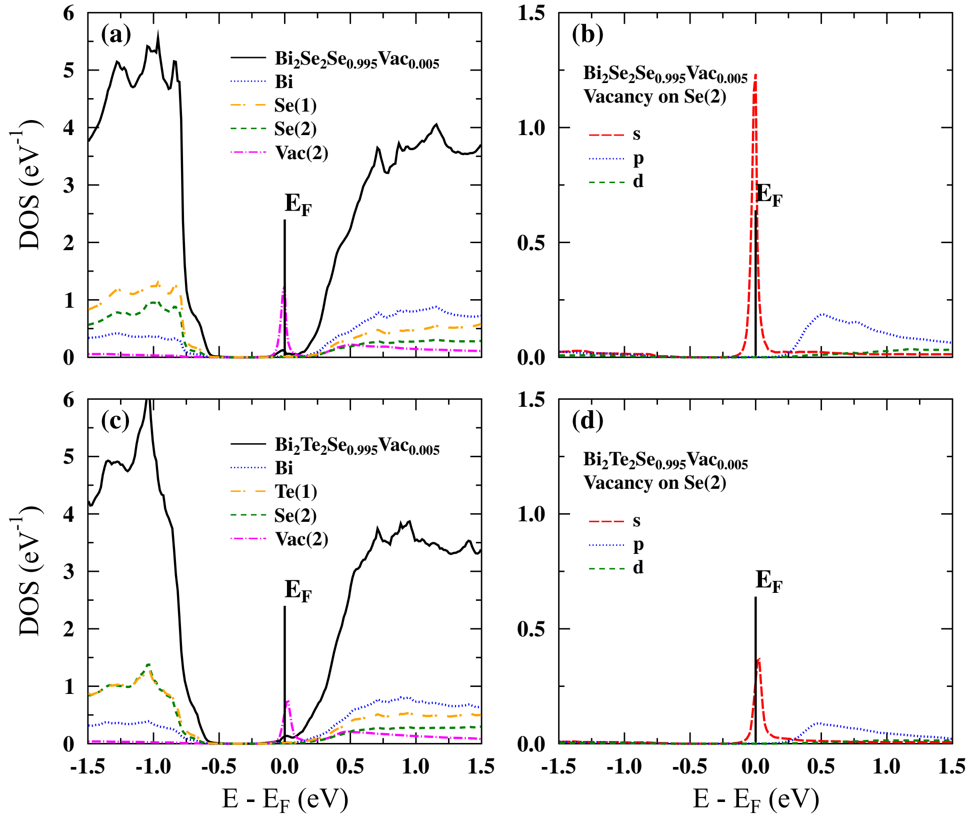

Fig. 6. Same as Fig. 5 but for vacancy located in the inner layer: (a) total DOS of $Bi_2Se_{2.995}$ containing 0.5% vacancies on Se(2), 1*a* crystal sites; (b) partial DOS at vacancy, decomposed over angular momentum; (c, d) same as (a, b) but for the $Bi_2Te_2Se_{0.995}$ case, containing 0.5% vacancies on Se(2) atom sites.

were carried out. The rhombohedral primitive cell was transformed into the hexagonal equivalent, containing three formula units (15 atoms), and the hexagonal unit cell was multiplied $2 \times 2 \times 1$ times, forming a 60-atom hexagonal supercell containing 12 Bi_2Te_3 formula units. A single Bi atom was then replaced by Sn, and resulting supercell had the *P3m1* space group (no. 156). The $Bi_{23}Sn_1Te_{36}$ supercell was then optimized, to investigate the lattice relaxation around the Sn impurity, in the semirelativistic approach and using the Perdew–Wang LDA.[42] We found only a small negative chemical pressure effect, which led to a decrease of the nearest- and next-nearest-neighbor distances around Sn (−1.6% and −0.5%, respectively). This is similar to what was observed in Sn-doped Bi.[41] For the relaxed supercell, computations including spin–orbit coupling (SOC) were carried out on a $10 \times 10 \times 3$ **k**-point mesh. The resulting densities of states are presented in Fig. 2, where one can see that the formation of the RL is generally not affected either by the relaxation process or by the spin–orbit coupling. This is partially due to the *s*-like nature of the resonance, confirmed in Fig. 2b. Although one should remember that the details of the band structure of the tetradymites do depend on spin–orbit coupling (especially the topological states), the larger-energy-scale effects, including the formation of the *s*-like RL, depend on SOC much more weakly. The exact position of the RL relative to the band edge may be altered by SOC, but the qualitative conclusion on the existence of the RL resulted independent of the SOC. A similar conclusion was established previously for Tl-doped PbTe,[29,40] and in the remainder of this work we rely on semirelativistic KKR–CPA results.

Having confirmed the formation of the RL in Bi_2Te_3 by Sn, we may now verify the resonant versus classical (rigid-band-like) behavior of Sn and other impurities in the tetradymite series of compounds. Figures 3 and 4 show the DOS of Sn-doped Bi_2Te_2Se and Bi_2Se_3, respectively. Similarly to the Bi_2Te_3 case, Sn forms a resonant peak, which becomes narrower and larger as Se substitutes Te. As in the previous case, the peak is *s*-like and accompanied by a hyperdeep state, below the valence band (not shown here). Figures 3b and 4b, where $x = 0.02$, show that also here Sn behaves as an acceptor, effectively doping the system *p*-type. Thus, according to our DFT–LDA calculations, Sn should be a resonant impurity also in Bi_2Te_2Se and Bi_2Se_3.

The literature concerning experimental studies on Bi_2Se_3:Sn is very limited; to the best of the

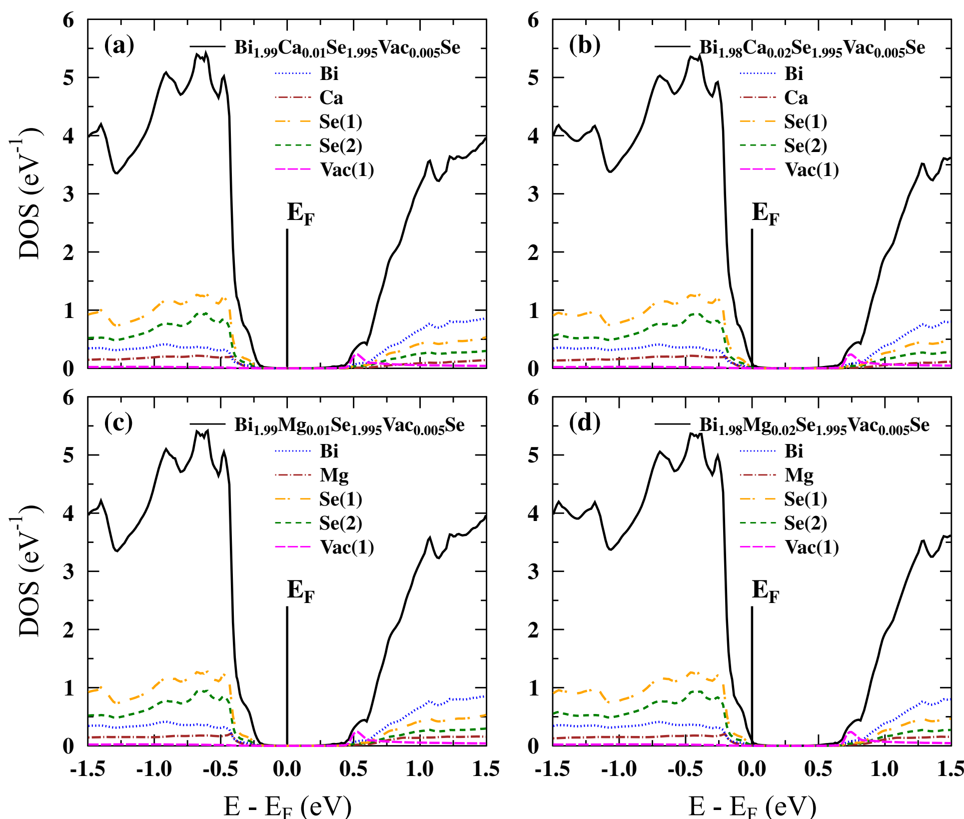

Fig. 7. DOS of Ca- (a, b) and Mg-doped (c, d) $Bi_2Se_{2.995}$ for the case where the vacancy is in the outer Se(1) layer. In (a) and (c), 1% Ca or Mg compensates the donor behavior of the 0.5% vacancies; for larger Ca/Mg concentrations, the material becomes *p*-type, as shown in (b, d).

author's knowledge, there is only one report, which classifies Sn as an acceptor.[43] Some more experimental data can be found on Bi_2Te_2Se:Sn, where Sn was also found to be an acceptor,[44–46] but no significant enhancement in thermopower due to Sn doping was found.[45] However, the situation in these two sister compounds is more complicated, compared with the Bi_2Te_3 case, due to the inseparable presence of a large amount of defects, which make both compounds naturally *n*-type.[2]

The thermoelectric properties of a series of Sn-doped Bi_2Te_2Se samples were investigated in Ref. 45, where it was suggested that the presence of 0.5% Se vacancies in $Bi_{2-x}Sn_xTe_2Se_{0.995}$ led to the simultaneous presence of *p*- and *n*-type carriers in the samples, resulting in a compensation effect, and $n - p$ crossover was observed while increasing x. For small Sn concentrations ($x \leq 0.005$), the samples were *n*-type, with relatively large thermopower and power factor. At around $x = 0.01$, the system was compensated (small Hall carrier concentration due to the opposite n and p components, the smallest S and PF in the series). For higher x, holes delivered by Sn started to dominate, and the sample with $x = 0.04$ was *p*-type, but the absolute values of S and PF were smaller, compared with the *n*-type samples. The authors summarized that work by saying that no evidence for the presence of a Sn resonant level was found, and that the Sn level might lie at lower energies, thus heavier *p*-type doping would have been required to observe RL effects. However, in two other works,[44,46] the presence of the impurity band related to the Sn resonant level was proposed, based on measurements of other physical properties and supercell electronic structure computations.

Se/Te Vacancies

To verify whether the formation of the resonant level on Sn may be altered by the presence of vacancies, one must perform electronic structure calculations for Bi_2Se_3 and Bi_2Te_2Se containing vacancies and impurity atoms simultaneously. We start our analysis by considering sole vacancies on chalcogen (Se, Te) atom sites, followed by more complex cases of doped and double-doped systems containing vacancies. In general, there are two possibilities for the location of chalcogen atom vacancies in the rhombohedral tetradymite. The first one is the vacancy in the "outer" (van der Waals) atomic layer, formed by Se(1) in Bi_2Se_3 and Te(1) in Bi_2Te_2Se, which we label in this work as Vac(1). The second one is the vacancy in the "inner" atomic layer, formed by Se(2) in Bi_2Se_3 and Bi_2Te_2Se, which we label in this work as Vac(2). Intuitively, the weakly bonded outer layer

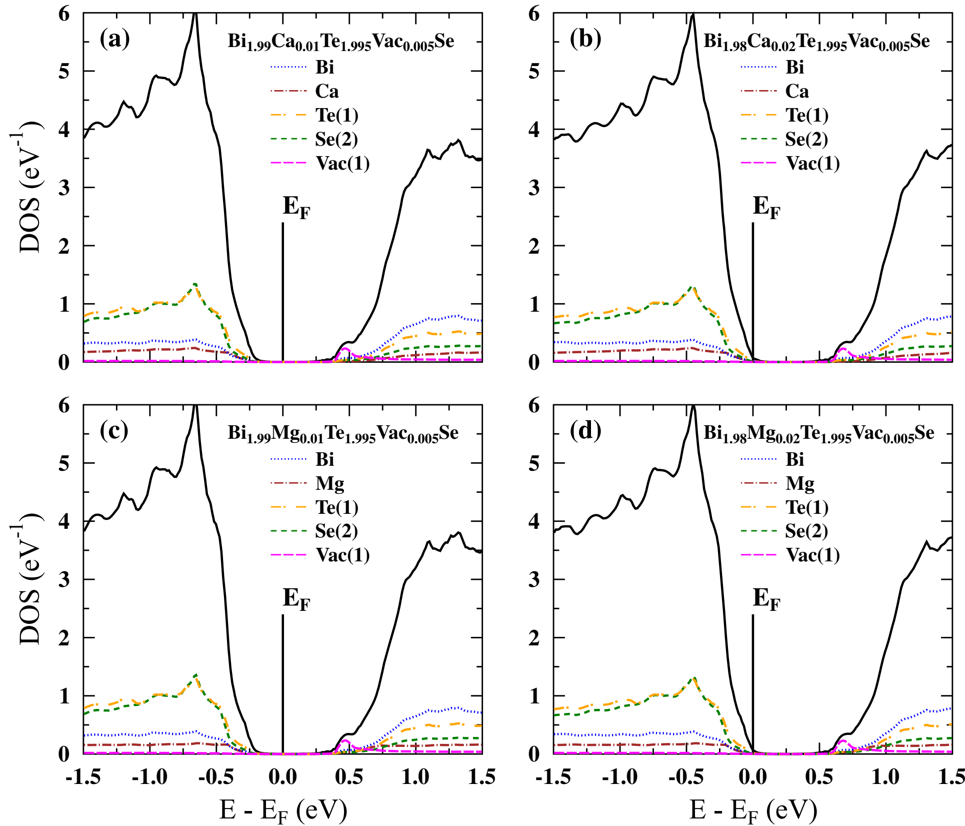

Fig. 8. DOS of Ca- (a, b) and Mg-doped (c, d) $Bi_2Te_{1.995}Se$ ("outer" layer Vac(1) case). In (a) and (c), 1% Ca and Mg compensates the donor behavior of 0.5% vacancies; for larger Ca/Mg concentrations, the material becomes *p*-type, as shown in (b, d).

should be more predisposed to contain vacancies. Theoretical studies on various types of defects in the tetradymites were recently reported,[47–49] generally confirming this prediction, i.e., that vacancies are more probable (at least under Bi-rich conditions) on Se(1) in Bi_2Se_3 and on Te(1) in Bi_2Te_2Se, rather than on Se(2). It is worth noting that the second prediction of the greater probability of vacancy formation on Te rather than on Se in Bi_2Te_2Se disagrees with the frequently discussed model.[2,45]

To make our results more general and independent of assumed vacancy location, in both Bi_2Se_3 and Bi_2Te_2Se, two possibilities of vacancy location were considered. As shown next, the most important observation is that the actual location of the vacancy is not critically important, especially if the material is desired to be *p*-type (and vacancies have to be counterdoped). The cumulative vacancy concentration per formula unit is the key parameter controlling the type of conductivity in the system.

Electronic structures of compounds with vacancies were calculated, using the same KKR–CPA method, as in the previous paragraph. Technically, a vacancy was simulated as an "empty sphere," i.e., an "atom" with $Z = 0$, placed on the selected site at the simulated concentration, and the electronic structure was then calculated self-consistently, using the coherent potential approximation.

First, we describe the more intuitive case of outer-layer vacancies, Vac(1). Figure 5a and b shows the DOS of Bi_2Se_3 with 0.5% vacancies on Se(1) atoms, whereas Fig. 5c and d presents the case of Bi_2Te_2Se with 0.5% vacancies on Te(1). First of all, the calculations correctly predict the *n*-type conductivity of the materials, with E_F located in the conduction band, as if the vacancies were electron donors. However, a rather striking feature is also observed in these figures, namely small bumps of the DOS created by the vacancies, seen in both cases. The partial DOS peaks on vacancies are several times smaller than the RL peaks on Sn atoms in these structures, but the vacancies still show non-rigid-band-like behavior, even forming resonant-like states, which may modify the electronic structure close to the conduction band edge.

Similar DOS peaks are observed for the second possible vacancy location, Vac(2), i.e., in the "inner" Se(2) atomic layer, as presented in Fig. 6. For this case, DOS peaks on vacancies are even larger and narrower, which might indicate that these crystal sites are not the preferred vacancy location, in agreement with the results of Refs. 47–49. Another difference between Vac(1) and Vac(2) becomes visible when comparing the angular momentum decomposition of the densities of states in Figs. 5b, d and 6b, d. The DOS peak at Vac(1), i.e., in the

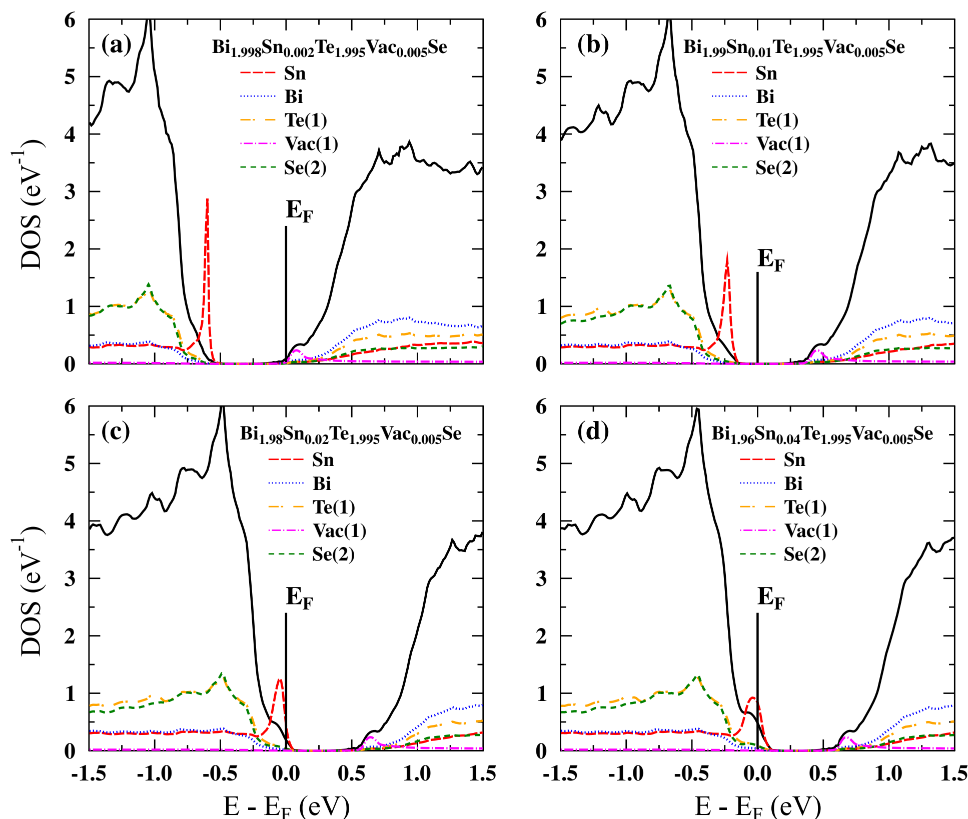

Fig. 9. Evolution of DOS and Fermi level position in $Bi_{2-x}Sn_xTe_{1.995}Se$: (a) $x = 0.002$, (b) $x = 0.01$, (c) $x = 0.02$, (d) $x = 0.04$. When the Sn concentration is larger than two times the vacancy concentration, E_F starts to penetrate the RL DOS peak (c), however for large concentrations (d), the RL peak becomes rather broad.

outer layer, has mainly *p*-like orbital momentum character, in contrast to the *s*-like states involved in the DOS peak at Vac(2). Nevertheless, the global effect of the presence of vacancies on the electronic structure is similar: both cases lead to *n*-type conductivity, and vacancies behave as charged donors (more precisely, two electron donors, as clarified in the next paragraph). For the present work and behavior of materials, which are designed to contain *p*-type RL impurities, such as Sn, compensation of these donors is required, and the difference between Vac(1) and Vac(2) is not important, as long as they do not alter the RL formation, which we address next. The key parameter, controlling the Fermi level position, is the total concentration of chalcogen vacancies, and the same number of additional acceptor atoms is required to compensate them, regardless of the site they occupy.

It is worth noting that this rather unexpected, resonant-like behavior of the vacancies remains in agreement with experimental studies, since the presence of resonant electronic states on Se vacancies in Bi_2Se_3 was earlier found experimentally, using scanning tunneling microscopy (STM).[50]

Our results show that vacancies may have a stronger than expected influence on the electronic structure of *n*-type Bi_2Se_3 and Bi_2Te_2Se, which may go beyond a simple rigid shift of the Fermi level into the conduction band. However, at present, it is difficult to judge whether vacancies have any considerable, positive or negative effect on the thermoelectric properties of these materials, since there are no vacancy-free samples with which to compare. Certainly, the mobility of electrons is expected to decrease slightly when vacancies are present in a sample, due to scattering on defects, which would degrade the thermoelectric performance. If any resonant-like, positive effect on the thermopower is associated with the local increase in DOS, we may expect that it should be relatively weaker than that due to the RL from Sn atoms, since the resulting DOS, associated with the vacancy, is considerably smaller. Thus, the balance between the drop in mobility against the (potential) gain in thermopower may result in a small effect on the PF. However, one cannot exclude that the relatively large values of the thermopower in *n*-type Bi_2Te_2Se containing vacancies are correlated with the formation of the “hump” in the DOS due to the presence of vacancies. Further experimental efforts on synthesis of vacancy-free samples would be required to draw any further conclusions.

Se/Te Vacancies Plus Regular Dopants

A successful approach for compensating vacancies, tuning the Fermi level, and making Bi_2Se_3

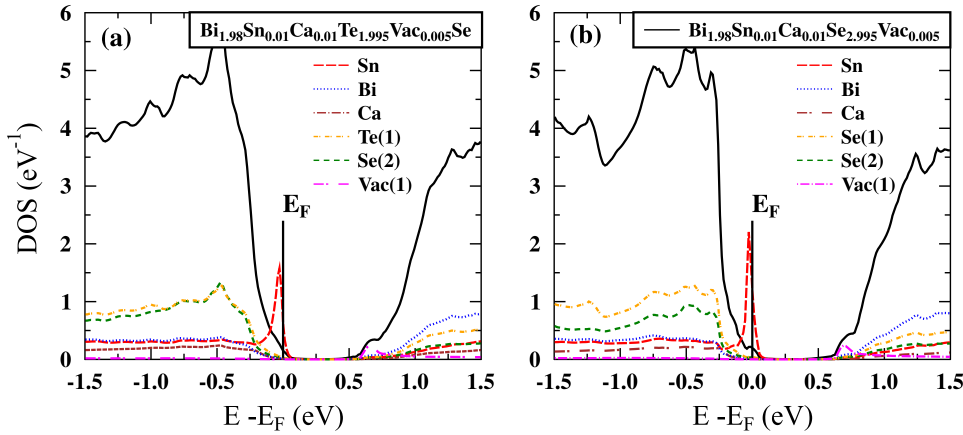

Fig. 10. DOS of doubly Sn/Ca-doped (a) Bi_2Te_2Se, and (b) Bi_2Se_3, both containing 0.5% of outer-layer vacancies Vac(1). Our results show that double doping, using a rigid-band-like acceptor (here Ca), should be an effective way of tuning the Fermi level position, without broadening the Sn RL too much.

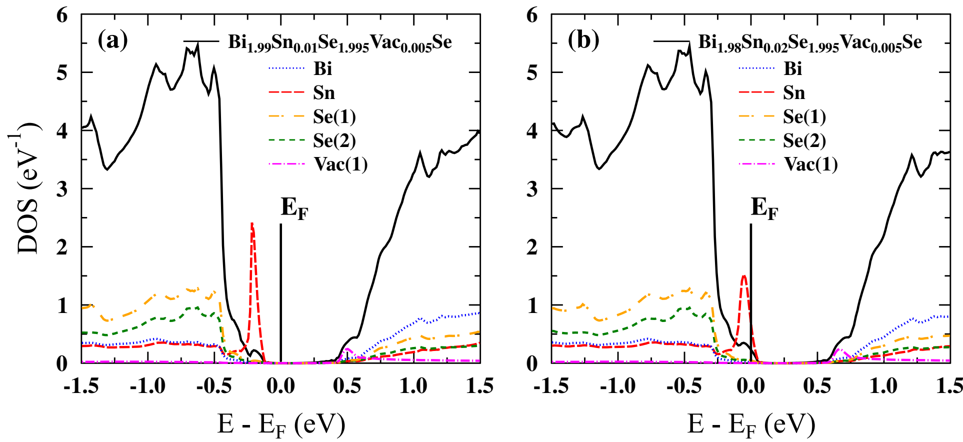

Fig. 11. Evolution of DOS and Fermi level position in Sn-doped $Bi_2Se_{2.995}$ for the case where the vacancy is on Se(1) atoms, i.e., "outer layer" Vac(1). When the Sn concentration is two times the vacancy concentration (a), the material is compensated. For larger concentrations (b), E_F is in the valence band but the RL peak broadens.

p-type was recently established to be doping with Ca,[4] Mg,[51] or Mn[52,53] on Bi site. Since Mn, with its open 3*d* shell and magnetic properties, would require a separate discussion, in this work only the two alkaline-earth elements are studied. Our calculation results for the Ca- and Mg-doped systems containing vacancies in the outer layer [Vac(1)] are presented in Fig. 7 for Bi_2Se_3 and Fig. 8 for Bi_2Te_2Se. The same set of figures for vacancies in the inner layer [Vac(2) case] are presented in the Appendix as Figs. 14 and 15, respectively. In all cases, Mg and Ca behave as regular acceptors, rigidly moving the Fermi level towards the valence band, without noticeable changes in the DOS of the doped materials. Both alkaline-earth elements behave as single-electron acceptors, delivering one hole per substituted atom. When the concentration of the dopant is equal to two times the concentration of vacancies (see Figs. 7, 8, 14, and 15), the material is compensated and E_F is located in the middle of the bandgap. For larger acceptor concentrations, effectively *p*-type material is obtained, in agreement with experiment, and for both Vac(1) and Vac(2) locations.

Se/Te Vacancies Plus Sn

Now the question arises of how the resonant state on Sn behaves when vacancies are present in the material. As mentioned above, the thermoelectric properties of Bi_2Te_2Se:Sn have been systematically investigated experimentally, and no substantial effect on the thermopower, due to the presence of Sn, was found.[45] Now, we try to reproduce that experiment and see how the electronic structure changes when Sn is added to the vacancy-containing compound. In Ref. 45, the authors assumed that the *n*-type behavior of the initial Bi_2Te_2Se material

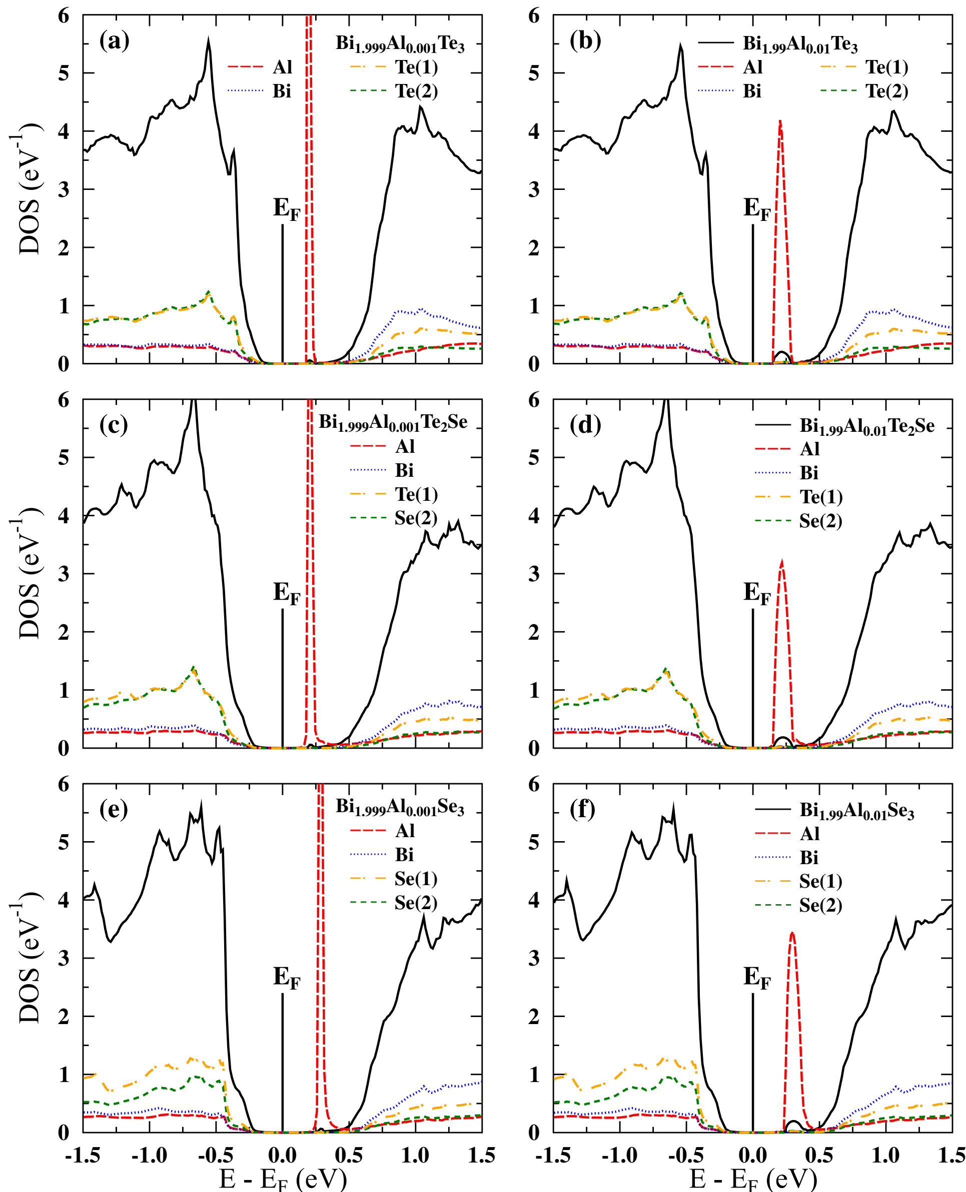

Fig. 12. DOS of Al-doped tetradymites: (a, b) Bi_2Te_3; (c, d) Bi_2Te_2Se; (e, f) Bi_2Se_3. The strongly peaked DOS shows the possibility of RL formation, but the E_F position is not sensitive to the concentration of Al, thus Al may be an electrically inactive impurity.

was due to the presence of 0.5% vacancies in the inner chalcogen layer [i.e., on Se(2) atoms, our Vac(2) case]. We show below that the material's behavior does not depend on this assumption, and similar changes in the transport properties of Bi_2Te_2Se could be observed if the vacancies were located in the outer layer of Te atoms.

As for previous analysis, we start by considering the more intuitive, outer layer vacancies [Vac(1)]. Figure 9 shows the evolution of the density of states of $Bi_{2-x}Sn_xTe_{1.995}Se$, i.e., for fixed 0.5% Te(1) vacancy concentration. In panel (a), for $x = 0.002$ of Sn, the system is n-type, and a large Sn resonant peak is present on the valence side of the bandgap. For $x = 0.01$ (Fig. 9b), the holes delivered by Sn lead to compensation of the donor vacancy effect, and E_F, as in the Ca and Mg cases, falls into the gap. Further increase of the tin concentration to $x = 0.02$ in panel (c) and $x = 0.04$ in panel (d) places E_F inside the valence band. The Sn concentration at which $n-p$ crossover takes place remains in very good agreement with experimental studies.[45] Exactly the same behavior is observed when the vacancy occupies the inner (Se) atomic layer (see Appendix, Fig. 16).

From our calculations we see that the formation of the RL on Sn is not disturbed by the presence of vacancies, and E_F should penetrate the DOS region, where the RL from Sn is present also for the 4% Sn-doped sample studied in Ref. 45. The problem that

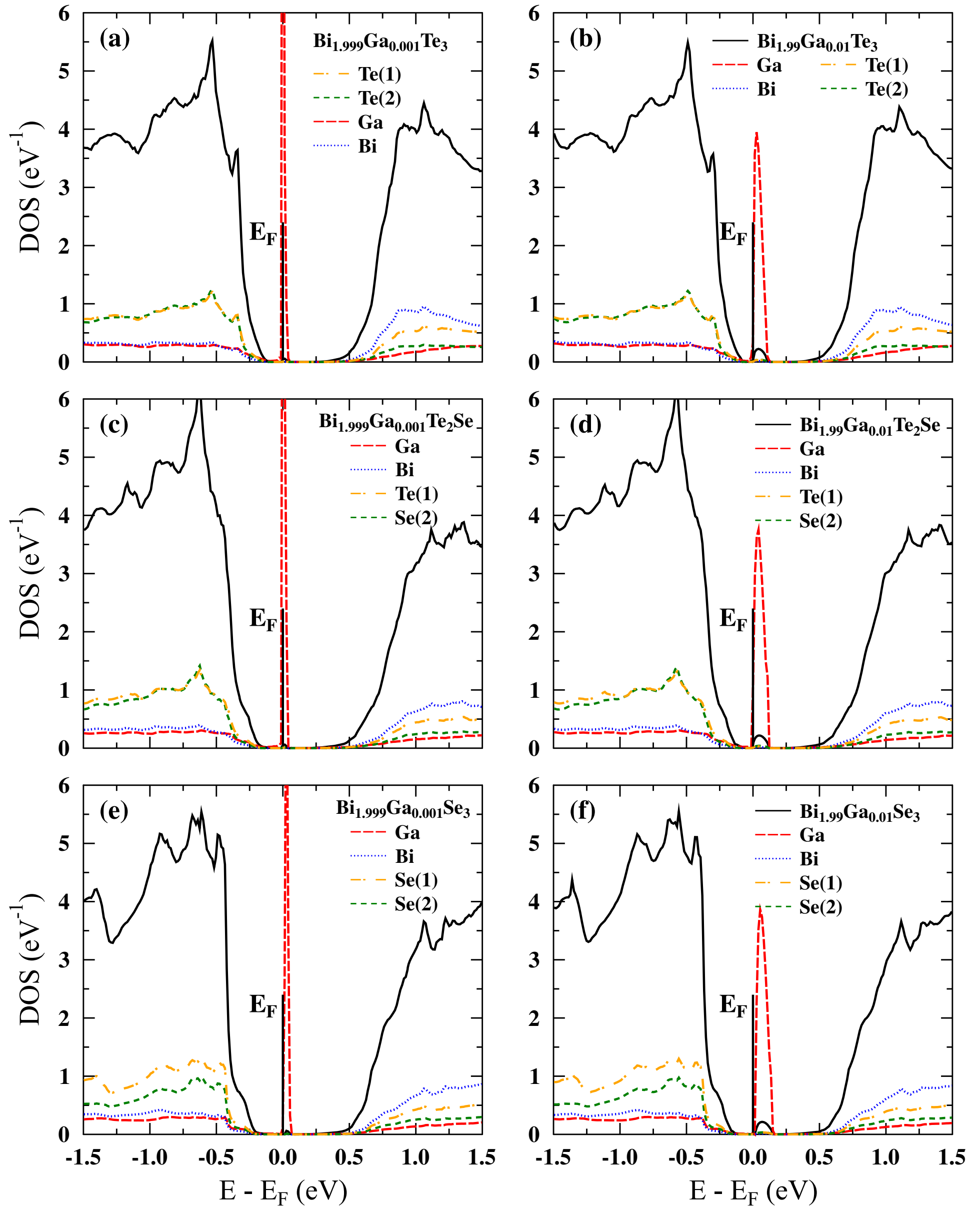

Fig. 13. DOS of Ga-doped tetradymites: (a, b) Bi_2Te_3; (c, d) Bi_2Te_2Se; (e, f) Bi_2Se_3. Similarly to Al, the strongly peaked DOS shows the possibility of RL formation, and the position of E_F does not change with the Ga concentration. If the position of the Ga level is correctly predicted by LDA calculations, the possibility that the impurity forms a trap state in the gap is larger for Ga than for Al.

the RL effect was not observed in the thermopower measurements may be related to the large concentration of Sn used in that experiment. Earlier studies on Bi_2Te_3:Sn, as mentioned in Sect. "Sn Resonant Level", showed that the Sn concentration has to be tuned precisely in order to observe the increase of thermopower. In Bi_2Te_3:Sn, this was done for $1\% \leq x \leq 2\%$, and for the larger Sn concentration of $x = 5\%$, the increase in thermopower was no longer evident. In Ref. 45, the authors had to heavily dope the samples with tin to overcome the n-type behavior driven by defects, and succeeded in obtaining a p-type sample for $x = 4\%$. It is possible that such a concentration may be too large to observe the positive effect of Sn on the thermopower, similarly to the 5% Sn-doped Bi_2Te_3; for too large amount of dopants, the RL may become too broad and the Sn may lose its resonant character, starting to behave as a typical acceptor.

We are now in a position to suggest, at least in principle, a simple way of resolving this problem. Instead of heavily doping the sample with Sn to reach the valence band, one can use regular acceptors, such as Ca or Mg, to compensate the n-type defects and tune the Fermi level position, keeping the Sn concentration constant at a lower level, say

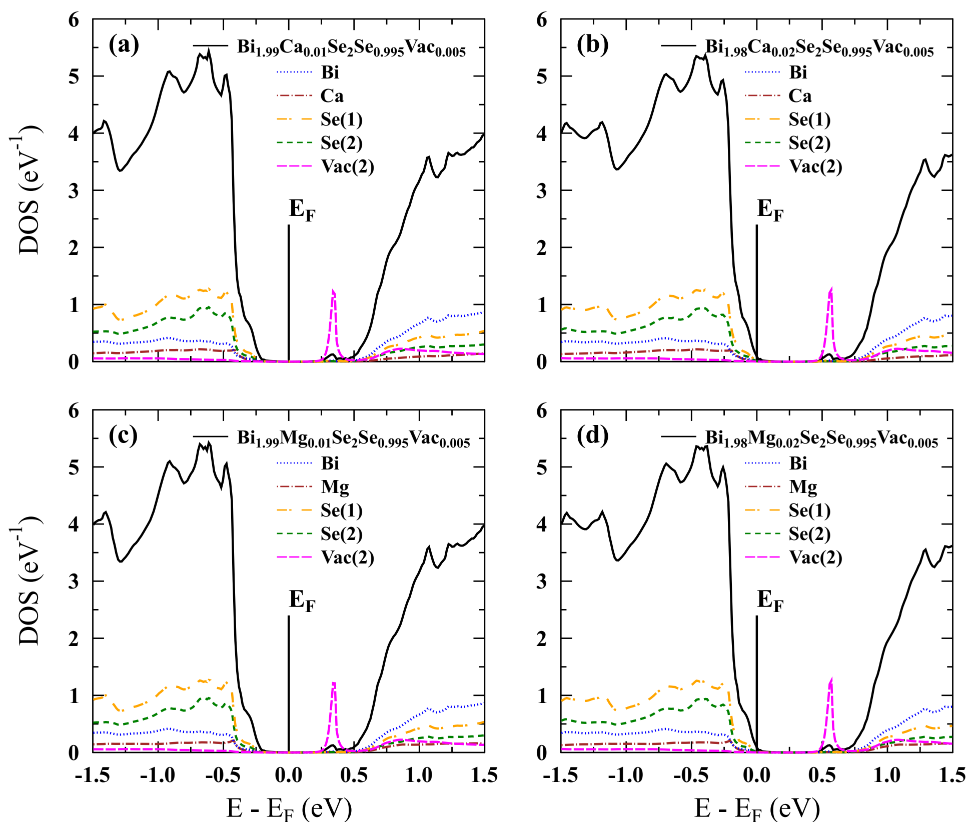

Fig. 14. "Inner layer" vacancy case for Ca- (a, b) and Mg-doped (c, d) $Bi_2Se_{2.995}$, i.e., containing 0.5% Se(2) vacancies. In (a) and (c), 1% Ca/Mg compensates the donor behavior of the 0.5% vacancies; for larger Ca/Mg concentrations, the material becomes *p*-type, as shown in (b, d). The E_F behavior is exactly the same as for the "outer layer" Vac(1) case, presented in Fig. 7.

between x = 0.5% and 2%. Measurements on such a series of doubly doped samples should clarify whether the Sn resonant level in Bi_2Te_2Se can be reached and whether it has a positive influence on the thermoelectric properties of the material. Figure 10a shows the DOS of such a doubly doped system, containing 0.5% Te vacancies: $Bi_{1.98}Sn_{0.01}Ca_{0.01}Te_{1.995}Se$. For the 1% Sn concentration and without Ca, the material would be compensated, as in Fig. 9b. Addition of 1% calcium shifts the Fermi level into the valence band, while Sn retains its substantial partial DOS peak, which is not smeared much, as would be observed for larger Sn concentration. Thus, double doping seems to be an efficient way of controlling the Fermi level position in the presence of vacancies and resonant level. Moreover, the same conclusion holds for the second possibility of the vacancy location; see, Fig. 18a in the Appendix for a similar DOS picture for the Vac(2) case.

As far as Bi_2Se_3 is concerned, we are not aware of any published experimental works on its thermoelectric properties upon Sn doping. Our computations show that, theoretically, the conclusions drawn above for Bi_2Te_2Se are also valid for vacancy-containing Bi_2Se_3, and the formation of the RL on Sn in DFT computations is independent of the presence of vacancies. The evolution of the DOS and Fermi level with increasing Sn concentration in $Bi_{2-x}Sn_xSe_{2.995}$ was found to be similar to the Sn-doped $Bi_2Te_{1.995}Se$ case (Fig. 9), thus in Fig. 11 we show only the DOS for the 1% and 2% Sn concentrations, where the material is compensated (a), and where *n*–*p* crossover takes place (b). Again, as for Bi_2Te_2Se, we show in Fig. 10b that the double-doping strategy may be used to effectively control the Fermi energy, keeping the Sn concentration at the level of 1% to 2%, where positive effects of the RL on the thermopower may be expected. These aforementioned observations do not change when the vacancy is located in the inner layer [Se(2) atoms, Vac(2) case], which is presented in Figs. 17 and 18b in the Appendix.

Al and Ga: Possible New Resonant Impurities

In this final section, we would like to suggest two new possible resonant impurities for the tetradymite series of materials, namely Al and Ga, to stimulate further experimental work on them. As far as literature reports are concerned, two works[54,55] reported anomalous increase of the thermopower and ZT in Ga-doped *n*-type $(Bi_{0.5}Sb_{0.5})_2Te_3$ alloy, which may be due to RL formation. Results of

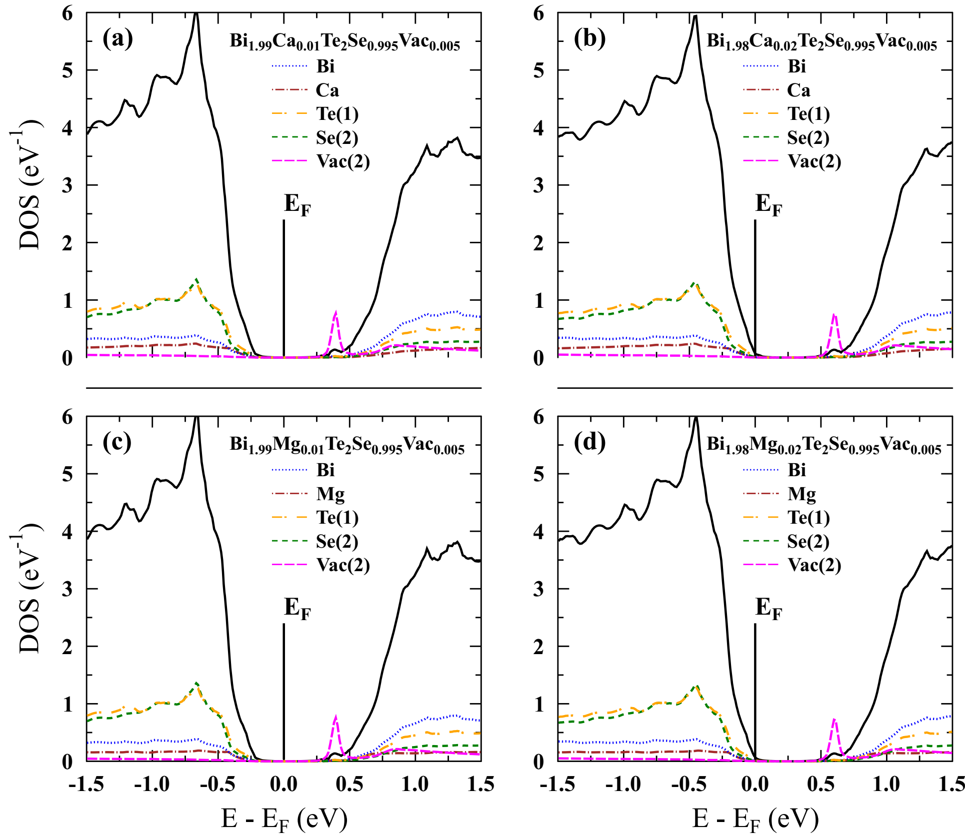

Fig. 15. "Inner layer" vacancy case for Ca- (a, b) and Mg-doped (c, d) $Bi_2Te_2Se_{0.995}$, i.e., containing 0.5% Se(2) vacancies. In (a) and (c), 1% Ca/Mg compensates the donor behavior of the 0.5% vacancies; for larger Ca/Mg concentrations, the material becomes *p*-type, as shown in (b, d). The evolution of the electronic structure is similar to the "outer layer" Vac(1) case, presented in Fig. 8.

the calculations for the series of Al- and Ga-doped materials are presented in Figs. 12 and 13.

For both Al (Fig. 12) and Ga (Fig. 13) impurities, and all of the host materials, we observe resonant peaks in the partial DOS of the impurity atoms. As in the Sn case, the DOS peaks are *s*-like, but several important differences are noticed. For the Al case, the resonant level is located at the edge of the conduction band (CB), and moves further towards the CB when the electronegativity of the neighboring atoms increases (from Te to Se). The evolution of the DOS with increasing Al concentration shows that, actually, Al is not changing the Fermi level position, which is located in the gap. Thus, Al seems to be an isoelectronic impurity, which can be understood as both Al and Bi are trivalent. Because of this, double doping with a second donor may be required to tune the Fermi level position and scan the resonant peak.

For Ga-doped materials (Fig. 13), the position of the Ga level is also in the gap, but closer to the valence band edge, compared with Al. Similarly to that case, we do not observe any shift in the Fermi level position when the concentration of the impurity is changed: E_F is rather pinned to the RL peak in the DOS within the gap. Also here, double doping with another donor would be needed to properly place E_F and investigate the Ga level. Partial substitution of Bi atoms with Sb may also affect these RL positions, since this would slightly modify the electronegativity of the cation site, as well as create chemical pressure. Both of these factors may influence the RL position.

The fact that Al and Ga impurities are isoelectronic with Bi in tetradymites may have an additional, positive effect on the thermoelectric performance. For such impurities, one may expect that the presence of Al or Ga would not induce any ionized impurity scattering, which would reduce the mobility of carriers in the system, but may additionally increase the thermopower via neutral impurity scattering, similarly as observed in In- and Ga-doped Bi.[41]

For these two dopants, we cannot directly compare our predictions with experiment, since the only measurements were reported for $(Bi\text{-}Sb)_2Te_3$ alloy, which we do not model here, but the possibility of the formation of the resonant level by Ga is strongly supported by the presented theoretical calculations. Additionally, we have to note that our calculations are

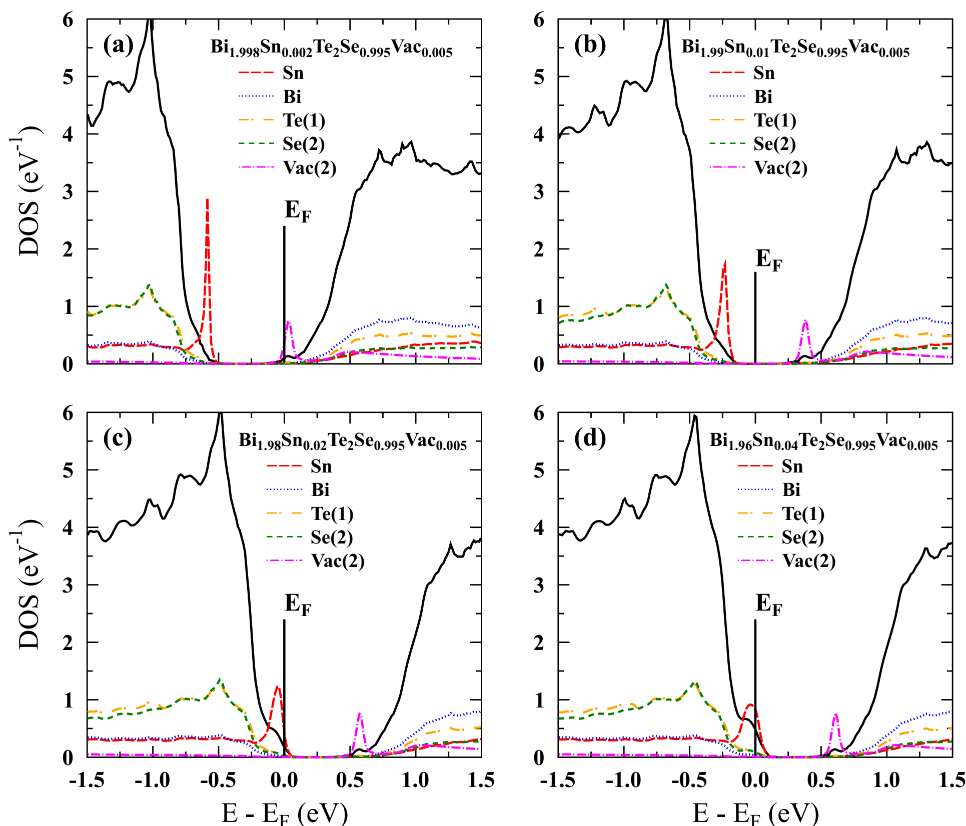

Fig. 16. Evolution of DOS and Fermi level position in $Bi_{2-x}Sn_xTe_2Se_{0.995}$, i.e., containing 0.5% "inner layer" Se(2) vacancies: (a) $x = 0.002$, (b) $x = 0.01$, (c) $x = 0.02$, (d) $x = 0.04$. When the Sn concentration is larger than two times the vacancy concentration, E_F starts to penetrate the RL DOS peak (c), however for large concentrations (d), the RL peak becomes rather broad. Results are similar to the "outer layer" vacancies case, presented in Fig. 9.

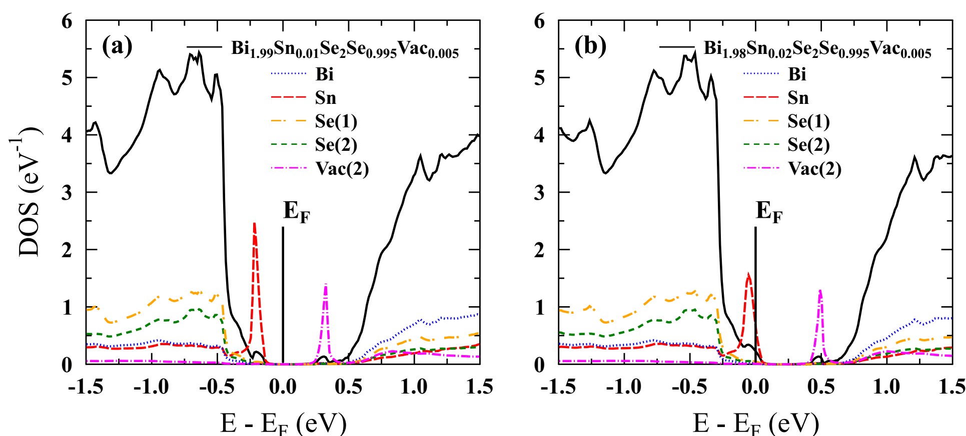

Fig. 17. Evolution of DOS and Fermi level position in Sn-doped $Bi_2Se_{2.995}$ for the "inner layer" Vac(2) case. E_F behavior and valence DOS are the same as for the Vac(1) case, presented in Fig. 11: when the Sn concentration is two times the vacancy concentration (a), the material is compensated. For larger concentrations (b), E_F is in the valence band but the RL peak broadens.

done using several approximations, including LDA, which may be not very accurate in predicting the exact position of the RL, especially for the case when it is above E_F. Here, the same problem occurs as for the bandgap value, and the mutual relation between the RL position and the conduction band edge is influenced by the inaccuracy of the gap. Thus, experimental verification of our predictions is highly desired.

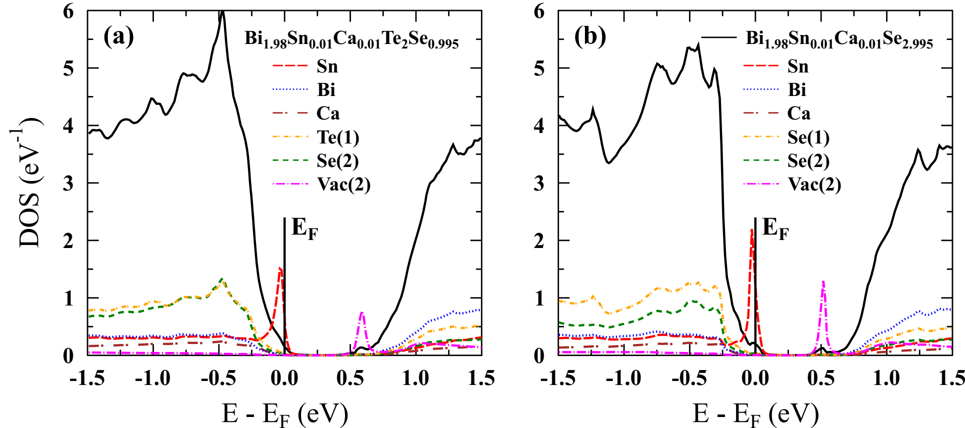

Fig. 18. DOS of doubly Sn/Ca-doped materials, containing 0.5% "inner layer" Se(2) vacancies: (a) Bi_2Te_2Se and (b) Bi_2Se_3. Similarly to the Vac(1) case (Fig. 10), our results show that double doping with rigid-band-like acceptor (Ca) should be an effective way of tuning the Fermi position without broadening the resonant level too much.

CONCLUSIONS

The results of first-principles calculations of the electronic structure of the tetradymites, Bi_2Te_3, Bi_2Te_2Se, and Bi_2Se_3, containing various impurities and vacancies, are presented. We found that Sn should be a resonant impurity in all the aforementioned materials, in agreement with experimental findings for Bi_2Te_3. Studies on Se-containing materials, i.e., Bi_2Te_2Se and Bi_2Se_3, showed that vacancies, which are very likely to be present in real samples, behave as charge donors and also create small, resonant-like peaks in the densities of states near the bottom of the conduction band. The angular momentum character of the DOS peaks on vacancies depends on the chalcogen atom site on which they are located, but the overall characteristics of the system, such as the sign of the majority carriers, depend only on the total vacancy concentration. Doping the Bi site with Ca or Mg, which was earlier experimentally shown to result in *p*-type materials, is theoretically confirmed as a rigid-band-like way of controlling the position of the Fermi level and turning the defected, *n*-type Bi_2Te_2Se and Bi_2Se_3 into *p*-type, with no major changes in the valence-band DOS. For Sn-doped Bi_2Te_2Se and Bi_2Se_3 containing vacancies, we showed that codoping of the material with Ca or Mg should be a better way of compensating the donor behavior of Te/Se vacancies, to reach the Sn resonant level, compared with heavy doping with Sn itself. This should help to avoid smearing of the resonant level, which is observed for larger Sn concentrations and through which the resonant character of Sn may be lost. Finally, we suggest Al and Ga as two new, potentially interesting impurities predicted to form resonant levels in the Bi-based tetradymites.

ACKNOWLEDGEMENTS

This work was partially supported by the Polish National Science Center (NCN) (Project No. DEC-2011/02/A/ST3/00124) and the Polish Ministry of Science and Higher Education.

OPEN ACCESS

This article is distributed under the terms of the Creative Commons Attribution 4.0 International License (http://creativecommons.org/licenses/by/4.0/), which permits unrestricted use, distribution, and reproduction in any medium, provided you give appropriate credit to the original author(s) and the source, provide a link to the Creative Commons license, and indicate if changes were made.

APPENDIX: A SECOND CHOICE OF THE LOCATION OF CHALCOGEN ATOM VACANCY SITE IN Bi_2Se_3 AND Bi_2Te_2Se

In this Appendix we present the DOS figures resulting from electronic structure calculations for doped Bi_2Se_3 and Bi_2Te_2Se containing vacancies in the "inner" Se(2) chalcogen atomic layer [our Vac(2) case]. Comparison with the figures included in Sect. "Results and Discussion" shows that the main results of this work do not depend on the position of the vacancy; i.e., we observe: (i) similar, two-electron-donor character of the vacancy, which forms small resonant-like peaks in the DOS; (ii) formation of RL at Sn also in the presence of vacancies; (iii) possibility of defect compensation upon doping with Mg and Ca, with the same acceptor concentration at the *n*–*p* crossover; (iv) successful tuning of the Fermi level position by double doping of moderately Sn-doped vacancy-containing materials, which helps to avoid the RL smearing effect, likely present for heavily Sn-doped samples. These results show that the vacancy concentration, not the vacancy location, is the key parameter for the properties of Bi_2Te_2Se and Bi_2Se_3, if one wishes to prepare *p*-type material.

Figure 14 shows the evolution of the DOS of Bi_2Se_3 containing vacancies on Se(2), when counterdoped using rigid-band-like acceptors Ca and Mg.

These two dopants allow one to compensate the donor behavior of the Se(2) vacancy in the same way as if the vacancy were located on Se(1) atoms (cf. Fig. 7). Similar conclusions are valid for Bi_2Te_2Se, when Figs. 8 and 15 are compared.

In Fig. 16, we observe that the evolution of the electronic structure for Sn-doped $Bi_2Te_2Se_{0.995}$, i.e., containing 0.5% "inner layer" Se(2) vacancies, when the concentration of Sn is increasing, is similar to that observed for the "outer layer" vacancy case (cf. Fig. 9).

Figure 17 shows results for Sn-doped $Bi_2Se_{2.995}$, with Se(2) vacancies. The DOS and *n*–*p* crossover, with increasing Sn concentration, are similar to those in Fig. 11 for Vac(1).

In Fig. 18, the *n*-type character of 0.5% Vac(2) material is compensated using a rigid-band-like acceptor (Ca) in the presence of RL at Sn atom in Bi_2Te_2Se (a) and Bi_2Se_3 (b), without broadening the Sn resonant level, in the same way as seen for the Vac(1) case in Fig. 10.

REFERENCES

1. G.J. Snyder and E.S. Toberer, *Nat. Mater.* 7, 105 (2008).
2. R.J. Cava, H. Ji, M.K. Fuccillo, Q.D. Gibson, and Y.S. Hor, *J. Mater. Chem. C* 1, 3176 (2013).
3. M.Z. Hasan and C.L. Kane, *Rev. Mod. Phys.* 82, 3045 (2010).
4. Y.S. Hor, A. Richardella, P. Roushan, Y. Xia, J.G. Checkelsky, A. Yazdani, M.Z. Hasan, N.P. Ong, and R.J. Cava, *Phys. Rev. B* 79, 195208 (2009).
5. H.J. Goldsmid, *Materials* 7, 2577 (2014).
6. L.P. Caywood and G.R. Miller, *Phys. Rev. B* 2, 3209 (1970).
7. H. Köhler, *Phys. Stat. Sol. (b)* 62, 57 (1974).
8. P. Pecheur and G. Toussaint, *Phys. Lett. A* 135, 223 (1989).
9. S.K. Mishra, S. Satpathy, and O. Jepsen, *J. Phys.: Condens. Matter* 9, 461 (1997).
10. P. Larson, V.A. Greanya, W.C. Tonjes, R. Liu, S.D. Mahanti, and C.G. Olson, *Phys. Rev. B* 65, 085108 (2002).
11. V.A. Greanya, W.C. Tonjes, R. Liu, C.G. Olson, D.Y. Chung, and M.G. Kanatzidis, *J. Appl. Phys.* 92, 6658 (2002).
12. E. Kioupakis, M.L. Tiago, and S.G. Louie, *Phys. Rev. B* 82, 1 (2010).
13. W. Zhang, R. Yu, H.J. Zhang, X. Dai, and Z. Fang, *New J. Phys.* 12, 065013 (2010).
14. I.A. Nechaev, R.C. Hatch, M. Bianchi, D. Guan, C. Friedrich, I. Aguilera, J.L. Mi, B.B. Iversen, S. Blügel, P. Hofmann, and E.V. Chulkov, *Phys. Rev. B* 87, 121111 (2013).
15. H. Scherrer, in *Materials, Preparation, and Characterization in Thermoelectrics*, ed. by D.M. Rowe (CRC Press, Boca Raton, 2012).
16. M.H. Francombe, *Br. J. Appl. Phys.* 9, 415 (1958).
17. S. Kaprzyk and A. Bansil, *Phys. Rev. B* 42, 7358 (1990).
18. A. Bansil, S. Kaprzyk, P.E. Mijnarends, and J. Tobola, *Phys. Rev. B* 60, 13396 (1999).
19. T. Stopa, S. Kaprzyk, and J. Tobola, *J. Phys.: Condens. Matter* 16, 4921 (2004).
20. H. Ebert, D. Ködderitzsch, and J. Minár, *Rep. Prog. Phys.* 74, 096501 (2011).
21. U. von Barth and L. Hedin, *J. Phys.: Condens. Matter* 5, 1629 (1972).
22. P. Blaha, K. Schwarz, G. Madsen, D. Kvasnicka, and J. Luitz, *WIEN2k, An Augmented Plane Wave + Local Orbitals Program for Calculating Crystal Properties* (Techn. Universität Wien, Austria, 2001).
23. V.A. Kulbachinskii, N.B. Brandt, P.A. Cheremnykh, S.A. Azou, J. Horák, and P. Lošták, *Phys. Stat. Sol. (b)* 150, 237 (1988).
24. M. Zhitinskaya, S. Nemov, and T. Svechnikova, *Phys. Solid State* 40, 1297 (1998).
25. C.M. Jaworski, V. Kulbachinskii, and J.P. Heremans, *Phys. Rev. B* 80, 233201 (2009).
26. J. Friedel, *Can. J. Phys.* 34, 1190 (1956).
27. J.P. Heremans, B. Wiendlocha, and A.M. Chamoire, *Energy Environ. Sci.* 5, 5510 (2012).
28. B.L. Györffy and G.M. Stocks, in *Electrons in Disordered Metals and Metallic Surfaces. NATO ASI Series, Physics, B42*, ed. by P. Phariseau, B.L. Györffy, and L. Scheive (Plenum Press, New York, 1979).
29. B. Wiendlocha, *Phys. Rev. B* 88, 205205 (2013).
30. B. Wiendlocha, *Appl. Phys. Lett.* 105, 133901 (2014).
31. S. Kim, B. Wiendlocha, H. Jin, J. Tobola, and J.P. Heremans, *J. Appl. Phys.* 116, 153706 (2014).
32. B. Wiendlocha, K. Kutorasinski, S. Kaprzyk, and J. Tobola, *Scr. Mater.* 111, 33 (2016).
33. J.D. König, M.D. Nielsen, Y.B. Gao, M. Winkler, A. Jacquot, H. Böttner, and J.P. Heremans, *Phys. Rev. B* 84, 205126 (2011).
34. J.P. Heremans, V. Jovovic, E.S. Toberer, A. Saramat, K. Kurosaki, A. Charoenphakdee, S. Yamanaka, and G.J. Snyder, *Science* 321, 554 (2008).
35. C.M. Jaworski, B. Wiendlocha, V. Jovovic, and J.P. Heremans, *Energy Environ. Sci.* 4, 4155 (2011).
36. Q. Zhang, H. Wang, Q. Zhang, W. Liu, B. Yu, H. Wang, D. Wang, G. Ni, G. Chen, and Z. Ren, *Nano Lett.* 12, 2324 (2012).
37. Q. Zhang, B. Liao, Y. Lan, K. Lukas, W. Liu, K. Esfarjani, C. Opeil, D. Broido, G. Chen, and Z. Ren, *Proc. Natl. Acad. Sci.* 110, 13261 (2013).
38. H.P. Hjalmarson, P. Vogl, D.J. Wolford, and J.D. Dow, *Phys. Rev. Lett.* 44, 810 (1980).
39. S. Ahmad, K. Hoang, and S.D. Mahanti, *Phys. Rev. Lett.* 96, 056403 (2006).
40. K. Hoang and S.D. Mahanti, *Phys. Rev. B* 78, 085111 (2008).
41. H. Jin, B. Wiendlocha, and J.P. Heremans, *Energy Environ. Sci.* 8, 2027 (2015).
42. J.P. Perdew and Y. Wang, *Phys. Rev. B* 45, 13244 (1992).
43. M. Matyáš, M. Závětová, J. Horák, and P. Lošták, in *Physics of Narrow Gap Semiconductors*, vol. 152, ed. by E. Gornik, H. Heinrich, and L. Palmetshofer (Springer, Berlin, 1982), pp. 405–409.
44. Z. Ren, A.A. Taskin, S. Sasaki, K. Segawa, and Y. Ando, *Phys. Rev. B* 85, 155301 (2012).
45. M. Fuccillo, S. Jia, M. Charles, and R. Cava, *J. Electron. Mater.* 42, 1246 (2013).
46. S.K. Kushwaha, Q.D. Gibson, J. Xiong, I. Pletikosic, A.P. Weber, A.V. Fedorov, N.P. Ong, T. Valla, and R.J. Cava, *J. Appl. Phys.* 115, 143708 (2014).
47. L.L. Wang, M. Huang, S. Thimmaiah, A. Alam, S.L. Bud'ko, A. Kaminski, T.A. Lograsso, P. Canfield, and D.D. Johnson, *Phys. Rev. B* 87, 125303 (2013).
48. D.O. Scanlon, P.D.C. King, R.P. Singh, A. de la Torre, S.M. Walker, G. Balakrishnan, F. Baumberger, and C.R.A. Catlow, *Adv. Mater.* 24, 2154 (2012).
49. D. West, Y.Y. Sun, H. Wang, J. Bang, and S.B. Zhang, *Phys. Rev. B* 86, 121201 (2012).
50. Z. Alpichshev, R.R. Biswas, A.V. Balatsky, J.G. Analytis, J.H. Chu, I.R. Fisher, and A. Kapitulnik, *Phys. Rev. Lett.* 108, 206402 (2012).
51. J. Androulakis and E. Beciragic, *Solid State Commun.* 173, 5 (2013).
52. Y.L. Chen, J.H. Chu, J.G. Analytis, Z.K. Liu, K. Igarashi, H.H. Kuo, X.L. Qi, S.K. Mo, R.G. Moore, D.H. Lu, M. Hashimoto, T. Sasagawa, S.C. Zhang, I.R. Fisher, Z. Hussain, and Z.X. Shen, *Science* 329, 659 (2010).
53. Y.B. Gao, B. He, D. Parker, I. Androulakis, and J.P. Heremans, *Phys. Rev. B* 90, 125204 (2014).
54. V.A. Kulbachinskii, V.G. Kytin, A.A. Kudryashov, and P.M. Tarasov, in *AIP Conference Proceedings* (2012), pp. 119.
55. V. Kulbachinskii, V. Kytin, P. Tarasov, and N. Yuzeeva, *Phys. Solid State* 52, 1830 (2010).